Energy Proceedings
Vol 30, 2023
ISSN 2004-2965

Hydrogen Production via Methane Steam Reforming with Simultaneous Separation of Hydrogen and Carbon Dioxide

Ke Guo[1,2], Mingkai Liu[2,3], Bin Wang[2,4], Yong Hao[2,4*]

1 Department of Thermal Science and Energy Engineering, University of Science and Technology of China, Hefei 230027, PR China

2 Institute of Engineering Thermophysics, Chinese Academy of Sciences, Beijing 100190, PR China

3 University of Chinese Academy of Sciences, Beijing 100049, PR China

4 Wu Zhonghua College, North China Electric Power University, Beijing 102206, PR China

* Corresponding Author. E-mail address: haoyong@iet.cn

ABSTRACT

Hydrogen has tremendous potential to bridge the energy transformation to a green and sustainable future. Steam methane reforming (SMR) is currently the primary means of hydrogen production, while it suffers from major barriers of high temperatures, high system complexity, and high CO_2 emission. To address such challenges, we propose separation-enhanced SMR driven by simultaneous separation of H_2 and CO_2 to reduce reaction temperature on the premise of ensuring high methane conversion for temperature ranges compatible with commercial solar parabolic trough collectors. Experimental and numerical studies both demonstrate methane conversion of >99% and high-purity hydrogen and CO_2 obtained at 400°C. Such low-energy penalty and low-carbon footprint approach shall enable promising solar hydrogen production by further integration with photovoltaic-powered separation and CO_2 sequestration.

Keywords: hydrogen, natural gas, low-carbon, simultaneous separation, decarbonization

NONMENCLATURE

Abbreviations	
SMR	Steam methane reforming
CSP	Concentrated solar power
S/C	Water-to-methane

1 INTRODUCTION

Solar energy, as an abundant and renewable energy source, is widely expected to play a crucial role in the alleviation of the global climate-change challenge and the realization of carbon neutrality targets. However, solar energy also has the common barriers of many other renewable energy sources, that is, low energy density, instability, and discontinuity in time and space. Such major hurdles in solar energy conversion and utilization can be bypassed by converting it into a high-energy density fuel. Hydrogen is a good choice to this end, and is expected to play a critical role in the undergoing energy transformation. Global hydrogen consumption is about 70 million tons per year currently, [1] accounting for about 2-5% of total energy consumption, of which 76% comes from natural gas [2, 3]. Steam methane reforming (SMR), the dominant approach of hydrogen production from natural gas, is a strongly endothermic reaction operated at high temperatures (800~1000°C), which is often a critical indicator of high energy demand, high energy loss and severe reaction conditions [4]. Thus dramatic reduction in the reaction temperature of SMR on the premise of ensuring high methane conversion not only means great savings in energy consumption and penalties (and moderate reaction conditions), but might also open up new possibilities of combining with low/mid- temperature concentrated solar power (CSP) technologies, such as the commercialized parabolic trough collectors (350~550°C) [5].

Product separation works by Le Chatelier's principle and effectively reduces the reaction temperature of SMR to different levels, depending on the specific method used to shift the chemical equilibrium forward. A few researchers have conducted methane reforming using membrane separators, which combine palladium (Pd) membrane with reactors to achieve simultaneous reaction and hydrogen separation. They applied the membrane reactors for methane reforming to explore lower reaction temperature [6], higher hydrogen purity [7], and a more compact SMR process [8]. Removing CO_2 can also shift the reaction in the direction of H_2

generation. Since J. R. Hufton et al [9] first proposed the sorption-enhanced reaction process in 1996, researchers have carried out extensive research on solid adsorbents that adsorb CO_2 in situ in the past 20 years [10, 11]. However, according to the stoichiometric ratio of the reforming reaction (Eq. 1), the enhancement effect of separating CO_2 on the reaction is far less than that of separating H_2. In addition, for single-product separation, the separation-entailed energy penalty will increase significantly while the separation enhancement effect increases weakly with the increase of separation degree, which makes it unlikely to achieve high methane conversion and low hydrogen production consumption at the same time.

In this work, a model of methane reforming with simultaneous hydrogen separation and in-situ capture of CO_2 is established, and the integrated solar PV- and CSE-driven SMR system is proposed. The kinetic model of the reaction is validated by experiments. The reaction temperature of SMR can be reduced to ~400°C with >99% of methane conversion, matching the temperature ranges of commercial solar parabolic trough collectors. For the hydrogen production system proposed, the first-law thermodynamic efficiency and net solar-to-fuel efficiency can reach as high as 67.83% and 30.80% at 400°C, a water-to-methane (S/C) ratio of 4, and 60 NmL min^{-1} of methane flow rate. Solar-driven SMR at low/mid- temperatures saves the consumption of methane fuel and further reduces the carbon footprint of the hydrogen production process. The carbon dioxide that can be traced back to the feedstock methane is completely captured for carbon sequestration or further utilization, thus approaching zero carbon emissions for hydrogen production.

2 REACTOR DESCRIPTION, MODELING AND EXPERIMENTAL VALIDATION

2.1 Reactor and system description

Steam methane reforming for H_2 production process contains three main reactions:

$$CH_4(g)+H_2O(g)\rightleftharpoons CO(g)+3H_2(g), \Delta H^{\ominus}_{25^{\circ}C}=+205.9\ \text{kJ mol}^{-1} \quad (1)$$

$$CO(g)+H_2O(g)\rightleftharpoons CO_2(g)+H_2(g), \Delta H^{\ominus}_{25^{\circ}C}=-41.1\ \text{kJ mol}^{-1} \quad (2)$$

$$CH_4(g)+2H_2O(g)\rightleftharpoons CO_2(g)+4H_2(g), \Delta H^{\ominus}_{25^{\circ}C}=+164.8\ \text{kJ mol}^{-1} \quad (3)$$

The reactor model of dual-separation SMR for hydrogen production is shown in Fig. 1(a). In the reactor, the Pd-Ag membrane and hydrotalcite are selected to achieve H_2 permeation and CO_2 adsorption respectively. Through the simultaneous separation of products (H_2, CO_2), the partial pressures of H_2 and CO_2 gradually decrease in a constant proportion, which is more conducive to promoting the forward movement of the reaction balance and also avoids the contradiction between high methane conversion and high energy penalty in the separation of single-product.

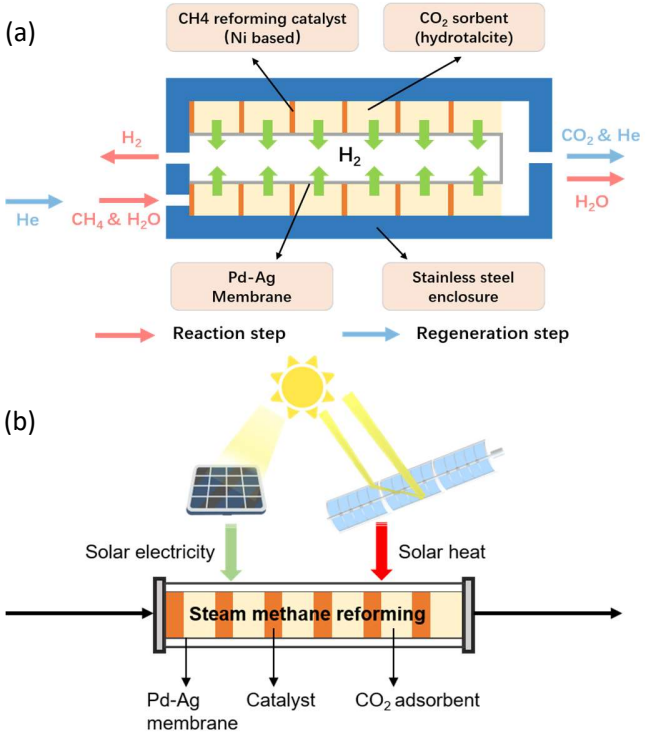

Fig. 1 (a) *Schematic diagram of the SMR reactor with H_2 separation and CO_2 adsorption (b) Schematic diagram of the integrated solar PV- and CSE-driven SMR system*

The dual-separation means facilitates the methane conversion, and can further reduce the reaction temperature of SMR to combine with solar concentrated heat. As shown in Fig. 1(b), the endothermic SMR is carried out at reduced temperatures, with solar collectors providing medium-temperature heat. The energy penalty consumed by the separation step is derived from solar photovoltaic electricity. The system converts unstable solar energy into the chemical energy of hydrogen, enabling solar-to-fuel conversion by combining it with fossil energy. For SMR, the addition of solar energy replaces the combustion of methane fuel, reducing methane consumption and CO_2 emission. The combination of SMR and solar energy will not only contribute to the decarbonization of methane reforming reactions, but also to the further development of solar energy.

2.2 Mathematical model

We establish a mathematical model to simulate the process of SMR with simultaneous-product separation. The model employs a 1D geometry for the reactor and

solves fully coupled equations for mass transport, energy transport, fluid motion, and chemical reaction in Comsol 5.5 [12]. The Ni catalyst and hydrotalcite sorbent can be approximated as a homogeneous packed bed with mm-size pores for the convenience of simulation. The key parameters of the model are shown in Table 1. To show the focus and make the logic well organized, we present the kinetic models of the individual processes emphatically, and the coupled equations for fluid motion, energy transport, and mass transport are not shown here. The following sections briefly describe the reaction kinetics, separation kinetics, and adsorption kinetics.

Table 1 Key parameters of the numerical model

Key parameters	Value	Units
Temperature, T	300-425	°C
Reaction pressure, P_0	10^5	Pa
Separation pressure, P_1	2000	Pa
Methane flow rate	60-200	ml min^{-1}
S/C ratio	2-6	
Diameter of Pd-Ag membrane tube	7	mm
Diameter of reactor	30	mm
Length of reactor	380	mm
Length of each catalyst segment	8	mm
Length of each sorbent segment	55.3	mm
The thickness of Pd-Ag membrane	3	μm
Sets of catalyst-sorbent combination	6	

For simplicity of analysis, only the three main reactions, i.e. Eq.s 1 to 3 are considered to take place in the reactor. Their reaction rates are expressed as follows [13]:

$$r_1 = \frac{k_1 P_{H_2}^{-2.5}\left(P_{CH_4}P_{H_2O} - P_{H_2}^3 P_{CO} K_{eq,1}^{-1}\right)}{DEN^2} \quad (4)$$

$$r_2 = \frac{k_2 P_{H_2}^{-1}\left(P_{CO}P_{H_2O} - P_{H_2}P_{CO_2} K_{eq,2}^{-1}\right)}{DEN^2} \quad (5)$$

$$r_3 = \frac{k_3 P_{H_2}^{-3.5}\left(P_{CH_4}P_{H_2O}^2 - P_{H_2}^4 P_{CO_2} K_{eq,3}^{-1}\right)}{DEN^2} \quad (6)$$

$$DEN = 1 + K_{H_2}P_{H_2} + K_{CH_4}P_{CH_4} + K_{CO}P_{CO} + K_{H_2O}\frac{P_{H_2O}}{P_{H_2}} \quad (7)$$

where k_j is reaction rate constant j; K_i is the adsorption constant of chemical species i; $K_{eq,j}$ is the equilibrium constant of reaction j; P_i is the partial pressure of chemical species i. The values of those parameters are shown in Table 2 [14].

In this study, the hydrogen permeation membrane is made of Pd-Ag membrane, and the hydrogen flux is determined by the diffusion coefficient, the concentration gradient and the thickness of membrane [15]:

$$J_{H_2} = \frac{k\left(P_{H_2,in}^n - P_{H_2,out}^n\right)}{d_M} \quad (8)$$

$$k = A\exp^{-\frac{E_A}{RT}} \quad (9)$$

where n is an exponent, and it equals 0.62 which fits well in the experiment between 350°C and 900°C [16], k is the rate constant, A is the pre-exponential factor, which is 3.21×10^{-8}, and $\exp^{-\frac{E_A}{RT}}$ is the fraction of collisions that have enough energy to react (i.e., have energy greater than or equal to the activation energy E_A, which equals to 13.41 kJ mol^{-1} in this work) at temperature T. In some other studies, the applicable temperature range of Eq. 8 is extended down to 27°C [17], and for simplicity of analysis and discussion below, we expand the temperature range from 300°C to 700°C reasonably.

A simple one-step linear driving force model with Elovich-type kinetic coefficient is adopted here to describe the high-pressure kinetics of K-MG30. The mathematic equations of the adsorption model are [18]:

$$\frac{dq}{dt} = k\left(q_e - q\right) \quad (10)$$

$$k = \begin{cases} k_a = r_a\left(\frac{p_{CO_2}}{p_0}\right)^c, \ q_e = q_{e,a} > q \\ k_d = r_d, \ q_e = q_{e,d} < q \end{cases} \quad (11)$$

The reaction rates r_a and r_d are calculated according to the Arrhenius form kinetic expressions：

$$r_a = A_a \exp\left(-\frac{E_a}{RT}\right) \quad (12)$$

$$r_d = A_d \exp\left(-\frac{E_d}{RT}\right) \quad (13)$$

The adsorption/desorption activation energy E_a and E_d are described by：

$$E_a = E_a^0 + \frac{gq}{q_{e,a}} \quad (14)$$

$$E_d = E_d^0 + \frac{gq}{q_{e,a}} \quad (15)$$

The fitted value of kinetic parameters is listed in Table 2. The flow in the membrane reactor is assumed as plug flow, and the major changes in partial pressure and conversion rates are distributed along the axial direction.

Table 2 Kinetics parameters of Ni-based catalyst for steam methane reforming

Parameters	Value	Units
k_1	$3.711\times10^{17}\,e^{\frac{-240.1\ kJ\ mol^{-1}}{RT}}$	(mol $Pa^{0.5}kg_{cat}^{-1}s$)
k_2	$5.431e^{\frac{-67.13\ kJ\ mol^{-1}}{RT}}$	(mol $Pa^{-1}kg_{cat}^{-1}s$)
k_3	$8.960\times10^{16}\,e^{\frac{-243.9\ kJ\ mol^{-1}}{RT}}$	(mol $Pa^{0.5}kg_{cat}^{-1}s$)
K_{H_2}	$6.12\times10^{-14}\,e^{\frac{82.90\ kJ\ mol^{-1}}{RT}}$	Pa^{-1}
K_{CH_4}	$6.65\times10^{-9}\,e^{\frac{38.28\ kJ\ mol^{-1}}{RT}}$	Pa^{-1}
K_{CO}	$8.23\times10^{-10}\,e^{\frac{70.65\ kJ\ mol^{-1}}{RT}}$	Pa^{-1}
K_{H_2O}	$1.77\times10^{5}\,e^{\frac{-88.68\ kJ\ mol^{-1}}{RT}}$	Pa^{-1}
$K_{eq,1}$	$1.198\times10^{23}\,e^{\frac{-26830\ K}{T}}$	Pa^{2}
$K_{eq,2}$	$1.767\times10^{-2}\,e^{\frac{4400\ K}{T}}$	Pa^{2}
$K_{eq,3}$	$K_{eq,1}K_{eq,2}$	Pa^{4}
E_a^0	489.33	kJ mol^{-1}
E_d^0	153.56	kJ mol^{-1}
g	369.37	kJ mol^{-1}
h	264.94	kJ mol^{-1}
A_a	1.837×10^{8}	s^{-1}
A_d	2475	s^{-1}
a	3.854	-
$q_{e,a}$	2	mmol g^{-1}
$q_{e,d}$	0	mmol g^{-1}

2.3 Experimental validation

We performed preliminary experiments of SMR to validate the mathematical model. The experimental device is shown in Fig. 2. Since this work mainly validated the reaction kinetics module, there is no membrane separation device in the reactor. The granular catalyst with a particle size of 1.9-2.4 mm is filled in the reactor with an inner diameter of 30 mm and length of 380 mm. The commercial Ni/MgO-Al_2O_3 SMR catalyst (40 wt% Ni) is used to catalyze the global SMR reaction. An electric furnace is applied to provide controlled thermal energy at designated temperatures. Material parameters are shown in Table 3.

(a)  (b) 

Fig. 2 Electric furnace experimental system. (a) Control console (b) Reactor

Table 3 Parameters of SMR catalyst

	Materials	Volume (mL)	Mass (g)	Particle size （mm）
Catalyst	Ni/MgO-Al_2O_3	30	35	1.9-2.4

In the experiment, methane and steam are fed into the reactor at methane flow rate of 60 mL min^{-1} and 120 mL min^{-1}, and the S/C ratio of 4, and the global SMR reaction (Eq. 3) takes place over the Ni catalyst. The experiment was carried out at reaction temperature of 400°C (corresponding to the typical operating temperature of solar trough collectors). The exhaust is analyzed by mass spectrometer to quantitatively determine gaseous components.

2.4 Evaluation criteria

2.4.1 Reactor performance

The main factor for the reactor is methane conversion, which is defined as:

$$X_{CH_4} = \frac{F_{CH_4,in} - F_{CH_4,out}}{F_{CH_4,in}} \times 100\% \quad (16)$$

where $F_{CH_4,in}$ and $F_{CH_4,out}$ are the molar flow rate of methane inlet and outlet, respectively.

2.4.2 Performance of the system proposed

Mid-temperature SMR is realized through dual-product separation, making reaction temperature ranges compatible with commercial solar parabolic trough collectors. For the system proposed (fig. 1(b)), the first-law thermodynamic efficiency and the net solar-to-H_2 efficiency are examined. The first-law thermodynamic efficiency is defined as:

$$\eta_{HHV} = \frac{F_{H_2} \cdot HHV_{H_2}}{Q_{heat} / \eta_{abs} / \eta_{opt} + W_{PV} / \eta_{s\to e} + F_{CH_4} \cdot HHV_{CH_4}} \quad (17)$$

where F_{H_2}, F_{CO} and F_{CH_4} are the molar flow rate of H_2 separated and CH_4 consumed, respectively; HHV_{H_2} and HHV_{CH_4} are the molar amount of higher value of H_2 and CH_4, respectively; η_{abs}, η_{opt}, and $\eta_{s\to e}$ are absorption efficiency of CSP, the optical efficiency of the collector, photoelectric efficiency, taking as 0.9, 0.87 and 0.2, respectively; Q_{heat} is the heat needed for the system, including preheat heat of the reactants (CH_4, H_2O) and the reaction endothermic heat, and described as:

$$Q_{heat} = Q_{preheat} + Q_{\Delta H} \quad (18)$$

where

$$Q_{preheat} = F_{H_2O,in} \cdot \left(\int_{25^\circ C}^{100^\circ C} c_{p,H_2O(l)} dT + r + \int_{100^\circ C}^{T} c_{p,H_2O(g)} dT \right) + F_{CH_4,in} \cdot \int_{25^\circ C}^{T} c_{p,CH_4(g)} dT \quad (19)$$

$$Q_{\Delta H} = F_{CH_4} \cdot X_{CH_4} \cdot \Delta H_1 + F_{CO_2} \cdot \Delta H_2 \quad (20)$$

where $Q_{preheat}$ is the heat of preheating water and methane from 25°C to T; $c_{p,H_2O(l)}$, $c_{p,H_2O(g)}$ and $c_{p,CH_4(g)}$ are the specific heat of liquid water, vapor water, and methane at 1 atm, respectively; r is the molar latent heat of vaporization of water, equals to 40.873 kJ mol^{-1} at 100°C and 1 atm; $Q_{\Delta H}$ is the enthalpy change of steam methane reforming; , $F_{H_2O,in}$, F_{H_2} and F_{CO_2} are the molar flow rate of water inlet, H_2 and CO_2 generated. ΔH_1 and ΔH_2 are enthalpy changes of methane reforming (Eq. (1)) and water gas conversion (Eq. (2)), respectively. W_{PV} is the pumping power of the vacuum pump that maintains low pressure on the hydrogen separation side, described as:

$$W_{PV} = F_{H_2} RT \ln\left(\frac{P_0}{P_1}\right) / \eta_{pump} \quad (21)$$

where P_0 is reaction pressure; P_1 is the pressure of the hydrogen separation side; η_{pump} is pump efficiency, taken as 0.28 [19].

To further examine the fraction of the chemical energy obtained (H_2) that comes from solar energy, we define the net solar-to-hydrogen efficiency:

$$\eta_{HHV,net} = \frac{F_{H_2} \cdot HHV_{H_2} - F_{CH_4} \cdot HHV_{CH_4}}{Q_{heat} / \eta_{abs} / \eta_{opt} + W_{PV} / \eta_{s\to e}} \quad (22)$$

3 RESULTS AND DISCUSSION

3.1 Model validation

According to the experiments set up above, methane conversion under different flow rates is calculated based on the inlet and outlet gaseous components measured. Comparing the experimental results with the simulation results of the established mathematical model (Fig. 3), it can be seen that the fitting degree is excellent with a maximum error of less than 2%, which validates the reliability of the model. The separation kinetics of palladium membrane [15] and the adsorption kinetics model of hydrotalcite [18] are derived from the literature, and will not be validated separately here. Subsequent simulation calculations are carried out based on this model. The calculated temperature in this paper is 400°C and the S/C ratio is 4 unless otherwise stated.

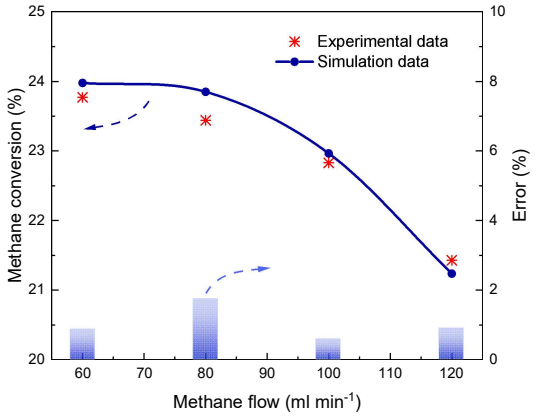

Fig. 3 Calibration of the mathematical model established with experimental data

3.2 The reactor performance under different working conditions

In the simulation, hydrogen is directly separated by Pd-Ag membrane, while carbon dioxide is separated by hydrotalcite adsorption. Therefore, the operation of the reactor includes a reaction step and a regeneration step. In the reaction step, methane and steam are fed into the reactor, and SMR reaction takes place over the Ni catalyst. Under vacuum conditions, the H_2 produced is separated from the reactor through the Pd-Ag membrane, and the CO_2 produced is simultaneously captured by the hydrotalcite adsorbent. In this work, hydrogen separation pressure is 2000 Pa. In the regeneration step, helium is used as a sweep gas to desorb CO_2 from the hydrotalcite sorbent at 1000 mL min^{-1} (standard conditions). Each cycle consists 1 min of reaction step and 2 min of regeneration step.

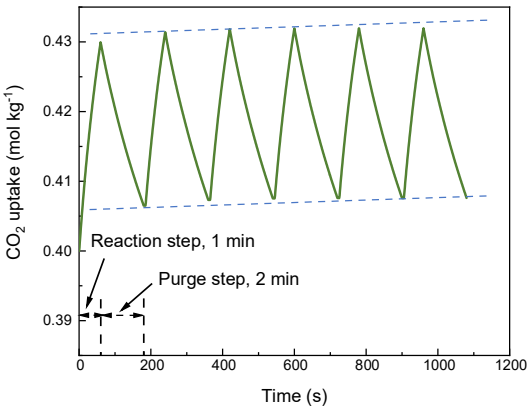

Fig. 4 CO_2 adsorption/desorption performance under cycles

Firstly, six cycles were calculated to investigate the adsorption and regeneration properties of the adsorbent. Theoretically, hydrotalcite can be completely desorbed after a long enough period. But in practice, the desorption time is not unlimited. In this work, we assume that the remaining CO_2 uptake after one cycle is set as 0.4 mol kg^{-1}. At the reaction step, the CO_2 uptake increases with the reaction process. At the purge step, CO_2 adsorbed by hydrotalcite is gradually released, and CO_2 uptake is gradually reduced. At the end of each purge step, the CO_2 uptake of hydrotalcite is lower than 0.41 mol kg^{-1}, indicating that it has good cycle characteristics.

From Fig. 5(a), methane conversion is higher at higher reaction temperatures, which is determined by the endothermic reaction characteristics of SMR. With the aid of dual-product separation, near-complete conversion of methane can be achieved at a temperature of 400°C. The pure hydrogen outlet flow rate follows the same trend as the methane conversion. When the temperature is greater than 400°C, the pure H_2 outlet flow is >235ml min^{-1}, meaning that the reaction achieves the maximum H_2 production and almost complete H_2 separation. Figure 5(b) shows the effect of reaction temperature on the thermodynamic efficiency of the system. The thermodynamic efficiencies increase significantly in the low-temperature section (300°C - 350°C) and level off when the temperature is > 350°C, which is mainly determined by the methane conversion. All reactants

entering the reaction are preheated, and the preheated energy for reactants that are not reacted is wasted at low methane conversions. At a temperature of 400°C, the first-law thermodynamic efficiency reaches a maximum of 67.83%, corresponding to the net solar-to-H_2 efficiency is 30.80%. And the efficiencies can be further improved when heat recovery is considered.

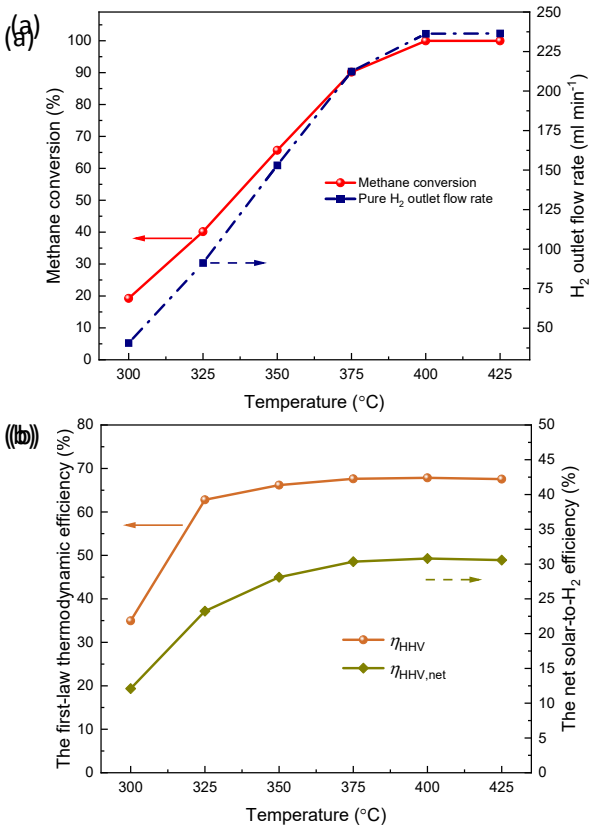

Fig. 5 System performance under different reactor temperatures. (a)Methane and H_2 flow rate (b) Thermodynamic efficiencies

The performance of the hydrogen-product system under different S/C ratios is calculated, as shown in Fig. 6. Methane conversion increases gradually with the increase of S/C and reaches >95% at 3 of S/C, which benefits from the dual-products separation. In Fig. 6(b), the S/C has almost no effect on the thermodynamic efficiency, mainly because only the reacted methane is considered in the efficiency calculation (the unreacted methane in the outlet is assumed to continue to be used), while the energy of the preheated water is small compared to the heat value of the methane. In the actual methane reforming process, water is often excessive, which can not only improve the methane conversion, but also prevent carbon deposition. However, the energy required for preheating water will increase with the increase of S/C, which will reduce the overall energy efficiency. Dual-product separation enables us to achieve high methane conversions at low S/C ratios. In this work, the S/C is taken as 4.

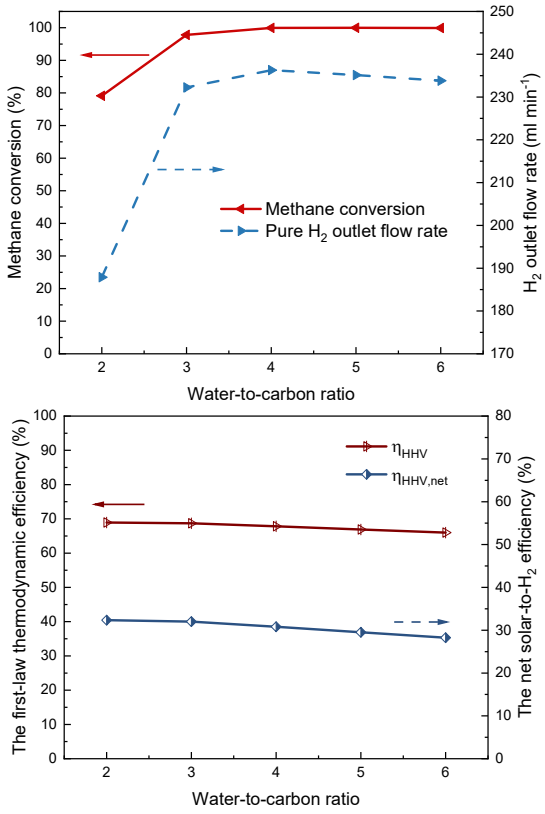

Fig. 6 System performance under different S/C ratios. (a)Methane conversion and H_2 flow rate (b) Thermodynamic efficiencies

The methane flow rate also affects the reaction performance, which should be considered comprehensively with the reactor size, catalyst and adsorbent loading capacity, and the separation capacity of Pd-Ag membrane. In Fig. 7(a), methane conversion decreases with increasing methane flow rate, which is determined by reaction kinetics, adsorption kinetics, and Pd-Ag membrane separation kinetics. The increase of pure H_2 outlet flow rate is due to the increase in inlet reactants, but in reality the amount of hydrogen produced per unit of methane is reduced, e.g. the ratio of hydrogen production to inlet methane is about 4 at 60 ml min^{-1} of methane flow but about 3 at 200 ml min^{-1} of methane flow. The energy efficiency decreases with increasing methane flow rate, which is related to the decrease in methane conversion, for the reasons explained above.

Figure 8 illustrates the composition of the energy sources per kJ of hydrogen produced by the solar-driven dual product separation hydrogen production pathway under 400°C, 4 of S/C, and 60 ml min^{-1} of methane flow rate. As you can see from Fig. 8, methane is still the largest part of the energy source, which is an inevitable feedstock consumption to produce hydrogen. In the hydrogen production system proposed, solar heat is mainly applied to preheat the reactants and provide reaction heat, and

solar PV electricity is mainly used to drive product separation. Solar energy replaces the consumption of methane fuel, which is beneficial for both energy conservation and the reduction of carbon emissions. On the other hand, the integrated solar PV- and CSE-driven SMR system realizes the conversion of intermittent, low energy-density solar energy to continuous, high energy-density chemical energy.

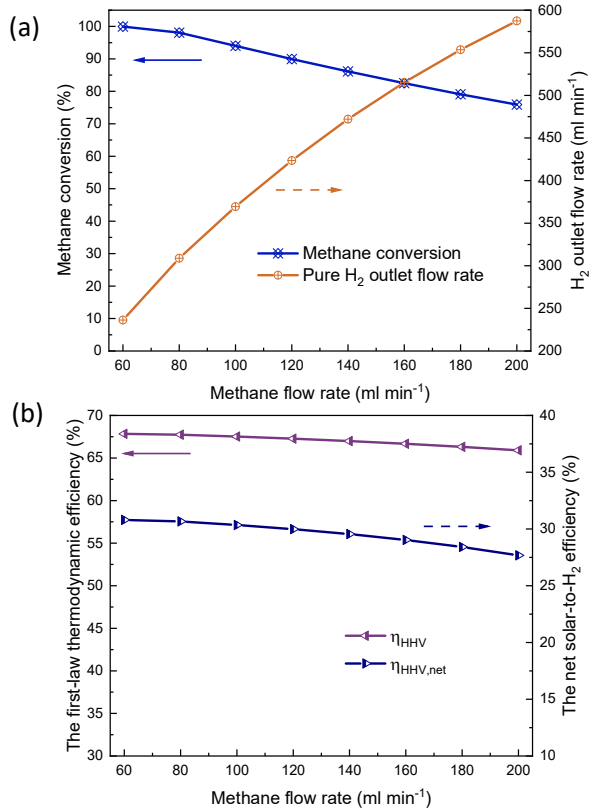

Fig. 7 System performance under different methane inlet flows. (a) Methane and H_2 flow rate (b)

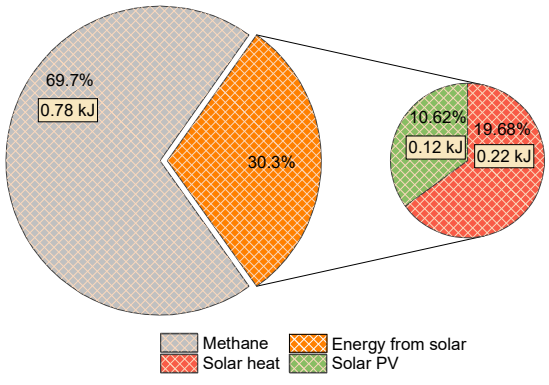

Fig. 8 Composition of energy consumption per kJ hydrogen produced

4 CONCLUSION

A simultaneous-product separation methane reforming reactor is proposed for efficient hydrogen production at low temperatures and a mathematical model is developed considering the kinetics of the reaction, separation, and adsorption. The reliability of the mathematical model is validated by experiments. Due to the dual-product separation, a methane conversion of >99%, high-purity hydrogen, and CO_2 is obtained at 400°C. The temperature ranges of dual-product separation SMR are compatible with commercial solar parabolic trough collectors and the electricity needed to separate H_2 can come from solar PV. The integrated solar PV- and CSE-driven SMR system is proposed and the hydrogen production performance is calculated. The first-law thermodynamic efficiency and net solar-to-fuel efficiency can reach as high as 67.83% and 30.80% under 400°C, 4 of S/C ratio, and 60 ml min^{-1} of methane flow rate. The system realizes the low temperature and decarbonization of methane reforming for hydrogen production and converts discontinuous solar energy to stable chemical energy with high-energy density. The new approach provides a viable low-temperature and efficient route to solar hydrogen production.

ACKNOWLEDGEMENT

This work is supported by the Basic Science Center Program for Ordered Energy Conversion of the National Natural Science Foundation of China (No. 51888103), and the joint research center for multi-energy complementation and conversion.

REFERENCE

[1] International energy agency (IEA). The future of hydrogen. 2019.

[2] Saavedra J, Whittaker T, Chen Z, et al. Controlling activity and selectivity using water in the Au-catalysed preferential oxidation of CO in H_2. Nat. Chem. 2016; 8: 584-589.

[3] Hosseini SE, Wahid MA. Hydrogen production from renewable and sustainable energy resources: Promising green energy carrier for clean development. Renew. Sust. Energ. Rev. 2016; 57: 850-866.

[4] Sinaei Nobandegani M, Sardashti Birjandi MR, Darbandi T, et al. An industrial steam methane reformer optimization using response surface methodology. J. Nat. Gas Sci. Eng. 2016; 36: 540-549.

[5] Khan J, Arsalan MH. Solar power technologies for sustainable electricity generation - A review. Renew. Sust. Energ. Rev. 2016; 55: 414-425.

[6] Giaconia A, Iaquaniello G, Caputo G, et al. Experimental validation of a pilot membrane reactor for hydrogen production by solar steam reforming of methane at maximum 550°C using molten salts as heat transfer fluid. Int. J. Hydrog. Energy 2020; 45: 33088-33101.

[7] Roses L, Gallucci F, Manzolini G, et al. Experimental study of steam methane reforming in a Pd-based fluidized bed membrane reactor. Chem. Eng. J. 2013; 222: 307-320.
[8] Ryi S-K, Park J-S, Kim D-K, et al. Methane steam reforming with a novel catalytic nickel membrane for effective hydrogen production. J. Membr. Sci. 2009; 339: 189-194.
[9] Carvill BT, Hufton JR, Anand M, et al. Sorption-enhanced reaction process. AIChE Journal 1996; 42: 2765-2772.
[10] Yong Z, Mata V, Rodrigues ArE. Adsorption of carbon dioxide at high temperature—a review. Sep. Purif. Technol. 2002; 26: 195-205.
[11] Ding Y, Alpay E. Equilibria and kinetics of CO2 adsorption on hydrotalcite adsorbent. Chem. Eng. Sci. 2000; 55: 3461-3474.
[12] COMSOL Multiphysics® v. 5.5. cn.comsol.com. COMSOL AB, Stockholm, Sweden.
[13] Xu JG, Froment GF. Methane steam reforming, methanation and water-gas shift. 1. Intrinsic kinetics. Aiche J 1989; 35: 88-96.
[14] Roses L, Manzolini G, Campanari S. CFD simulation of Pd-based membrane reformer when thermally coupled within a fuel cell micro-CHP system. Int. J. Hydrog. Energy 2010; 35: 12668-12679.
[15] Wang HS, Liu MK, Kong H, et al. Thermodynamic analysis on mid/low temperature solar methane steam reforming with hydrogen permeation membrane reactors. Appl. Therm. Eng. 2019; 152: 925-936.
[16] Morreale BD, Ciocco MV, Howard BH, et al. Effect of hydrogen-sulfide on the hydrogen permeance of palladium–copper alloys at elevated temperatures. J. Membr. Sci. 2004; 241: 219-224.
[17] Wang HS, Hao Y, Kong H. Thermodynamic study on solar thermochemical fuel production with oxygen permeation membrane reactors. Int. J. Energy Res. 2015; 39: 1790-1799.
[18] Zhu XC, Shi YX, Cai NS. High-pressure carbon dioxide adsorption kinetics of potassium-modified hydrotalcite at elevated temperature. Fuel 2017; 207: 579-590.
[19] Marxer D, Furler P, Takacs M, et al. Solar thermochemical splitting of CO2 into separate streams of CO and O-2 with high selectivity, stability, conversion, and efficiency. Energy Environ. Sci. 2017; 10: 1142-1149.